Available online at www.sciencedirect.com

ScienceDirect

Advances in Space Research 67 (2021) 3228–3236

ADVANCES IN SPACE RESEARCH (a COSPAR publication)

www.elsevier.com/locate/asr

Polar caps and auroral zones under idealized axisymmetric magnetic fields

Angel O.U. Parentis [a], Bruno S. Zossi [b,c], Hagay Amit [d], Ana G. Elias [b,c,*]

[a] Departamento de Fisica, Facultad de Ciencias Exactas y Tecnologia (FACET), Universidad Nacional de Tucuman (UNT), Av. Independencia 1800, 4000 Tucuman, Argentina

[b] Laboratorio de Ionosfera, Atmosfera Neutra y Magnetosfera (LIANM), Facultad de Ciencias Exactas y Tecnología (FACET), Universidad Nacional de Tucuman (UNT), Av. Independencia 1800, 4000 Tucuman, Argentina

[c] INFINOA, CONICET-UNT, Av. Independencia 1800, 4000 Tucuman, Argentina

[d] CNRS, Université de Nantes, Nantes Atlantiques Universités, Laboratoire de Planétologie et de Géodynamique, Nantes, France

Received 21 October 2020; received in revised form 28 January 2021; accepted 2 February 2021
Available online 20 February 2021

Abstract

The geomagnetic field, modified by the solar wind, determines the shape, area and location of polar caps and auroral zones, among other magnetosphere and upper atmosphere characteristics. Since the field varies greatly with time it is of interest to analyze polar caps and auroral zones variations linked to magnetic field variations of intensity and pattern. Polar caps and auroral zones locations and areas for various single harmonic axial field configurations are obtained analytically assuming a simple magnetopause model. As the axial degree n increases, the polar caps and auroral zones total number, given by $n + 1$ and $2n$ respectively, also increase. However, their total areas decrease from a larger value in the case of an axial dipole to a minimum for an axial octupole ($n = 3$), and then increase for increasing degrees. The increasing rate is much higher in the auroral zones case to the point that it exceeds the dipolar value at $n = 5$ while in the polar caps case this occurs at $n = 8$. The absolute latitudes of the auroral zones and polar caps that reside around the geographical poles increase with axial degree. Our results represent an end-member case of the evolution of auroral zones and polar caps during polarity reversals if the transition involves axial dipole energy cascade to higher axial degrees. Evidence for such an energy transfer is found in the historical record of the geomagnetic secular variation.

Keywords: Polar caps; Auroral zones; Geomagnetic field; Reversal

1. Introduction

The Earth's magnetic field is dominated by a tilted geocentric dipole. Based on the International Geomagnetic Reference Field (IGRF version 12) model (Thébault et al., 2015) for the year 2020, the present-day geomagnetic dipole accounts for ~ 93% and ~ 39% of the total field power at Earth's surface and at the core-mantle boundary (CMB), respectively. The present-day geomagnetic dipole tilt is relatively small, about 10 degrees (Amit and Olson, 2008), i.e. the dipole field is predominantly axisymmetric. The remaining non-dipolar field also contains significant axial contributions. In the present-day non-dipole field, the ratio of axial to non-axial field powers at Earth's surface and at the CMB is ~ 0.30 and ~ 0.22, respectively. This measure of the axial field is one of the primary morphological characteristics of the geomagnetic field that serves to constrain Earth-like numerical dynamo models (Christensen et al., 2010).

The geomagnetic field varies greatly with time. In the past 180 years the geomagnetic dipole has been rapidly

* Corresponding author at: Laboratorio de Ionosfera, Atmosfera Neutra y Magnetosfera (LIANM), Facultad de Ciencias Exactas y Tecnología (FACET), Universidad Nacional de Tucuman (UNT), Av. Independencia 1800, 4000 Tucuman, Argentina.
E-mail address: aelias@herrera.unt.edu.ar (A.G. Elias).

https://doi.org/10.1016/j.asr.2021.02.003
0273-1177/

decreasing (Finlay, 2008) while the axial part of the non-dipole field has been increasing (Christensen et al., 2010). Over millennial timescales, the most drastic large-scale changes occur during polarity reversals. Although the dominance of a dipolar configuration during polarity transitions is possible (Amit et al., 2010), paleomagnetic studies suggest the prevalence of a non-dipolar transitional field (e.g. Merrill and McFadden, 1999).

The geomagnetic core field determines, in addition to several upper atmosphere and magnetosphere features, the polar caps and auroral zones characteristics. Auroral zones are belts around polar caps where energetic charged particles from the solar wind follow the geomagnetic field lines and reach the upper atmosphere, resulting in an area with maximum frequency of aurorae occurrences (Akasofu, 1983; Feldstein, 2016). They are oval shaped due to the deformation of the Earth's magnetic field by the solar wind. The inner limit of this oval is determined then by the boundary of the polar caps, which in turn correspond to the footprints of the highly stretched field lines, or tail lobe lines, which are termed "open" field lines (Alexeev, 2005; Milan, 2009).

The influence of the Earth's magnetic field secular variation on polar caps and auroral zones over decadal to centennial timescales have been studied by several authors. Recently, Tsyganenko (2019) showed that the displacement of auroral ovals during the last 5 decades is related to the geomagnetic eccentric dipole secular variation. Zossi et al. (2020) found that since 1900 the polar caps and auroral ovals have been expanding in the southern hemisphere, as expected due to the geomagnetic dipole decrease (Finlay, 2008); however, counter-intuitively, in the northern hemisphere since 1940 the auroral ovals have been shrinking. Closely linked to auroral zones, Smith et al. (2017) analyzed auroral electrojets variations using satellite data. They detected changes associated with Earth's magnetic field secular variation, most notably larger latitudinal variability in the northern hemisphere.

The impact of reversals on polar caps and auroral zones has also been explored. Siscoe and Chen (1975) deduced that for a pure axial dipole, the polar cap boundary latitude, λ_p, varies in terms of the magnetic dipole moment, M, according to $\cos(\lambda_p) \propto (1/M)^{1/6}$, that is it moves equatorward as M decreases. Vogt and Glassmeier (2001) and Glassmeier et al. (2004) derived a similar scaling law again considering a dipolar geomagnetic field. The inclusion of non-dipolar components, added to a reduced dipolar component, was considered by Siscoe and Sibeck (1980) who estimated their effects on auroral zones shape and geographical displacement. They still found two auroral zones, due to the dipolar dominance at the magnetopause height, but their shape becomes elongated towards lower latitudes compared to their morphology under a pure dipole field. More recently, Zossi et al. (2019) determined polar caps' locations and shapes for different magnetic field reversal scenarios including dipole collapse, dipole rotation and energy cascade. They found polar caps changes not only in position, shape and area, but their number varied as well.

In the present work we determine the impact of specific components of the geomagnetic field on polar caps and auroral zones considering a set of axisymmetric single harmonic configurations of degrees n = 1 to 8, which have the appeal of available precise analytical solutions. We will show that in the past 120 years all the non-dipole axial geomagnetic field harmonics of degrees n = 2 to 8 have been increasing in parallel to the decrease of the axial dipole. In addition, studying the impact of these axial fields on the polar caps and auroral zones is interesting because the non-dipolar axial components may represent parts of a transitional field during reversals when the axial dipole vanishes by definition.

The methodology is described in section 2 followed by the results in section 3. Our concluding remarks are discussed in section 4.

2. Methodology

Based on the analytical equations of magnetic field lines derived by Willis and Young (1987) for axisymmetric single harmonic configurations of any degree, combined with the magnetopause model proposed by Zossi et al. (2020), we analytically assess the corresponding polar caps and auroral zones locations and areas. This magnetopause model, termed "constant intensity", allows us to detect the geomagnetic field open lines that determine the auroral zones inner and outer boundaries. It basically consists in balancing the dynamic pressure of the solar wind and the magnetic pressure of the geomagnetic field (Beard, 1960) in all directions for mean quiet and disturbed times. This B^{tot} value is on average ~ 50nT during quiet solar conditions. Considering the simple model of Chapman and Ferraro (1931) for the subsolar magnetopause distance, the Earth's core field is half of this B^{tot} value. The surface in space then, where $B^{int} = 25$ nT (Earth's field) serves as a modelled magnetopause. That is, the internal magnetic field at every point of the magnetopause is 25 nT since this value is determined by the solar wind dynamic pressure, which we consider fixed for all the cases analyzed. This intensity value would occur at different positions depending on the field configuration. Every line between 90° of inclination and the line with $B^{int} = 25$ nT at its apex is cut by this surface and is therefore considered as an "open field line". For an Earth's centered axisymmetric magnetic field, polar caps and auroral zones obviously have circular (i.e. axisymmetric) shapes centered at the Earth's rotation axis.

Our procedure consists of three steps which are explained below. Finally, we describe the Gauss coefficients used for the non-dipole scenarios.

2.1. Field line equations for a single harmonic axial magnetic field

Our first step is to recall the magnetic field lines equations. Field lines for any magnetic field configuration

whose spherical components at a given point in space are (B_r, B_θ, B_ϕ), are determined by solving the following differential equation

$$\frac{dr}{B_r} = \frac{rd\theta}{B_\theta} = \frac{r\sin\theta d\phi}{B_\phi} \quad (1)$$

where (r, θ, ϕ) are the radial, co-latitude and longitude spherical coordinates. Eq. (1), in the case of a single axisymmetric magnetic harmonic of degree n, has an analytic solution (Willis and Young, 1987):

$$r = r_n\left|\sin\theta P_n^1(\cos\theta)\right|^{1/n} \quad (2)$$

where r_n is an integration constant specifying a degree-dependent axisymmetric shell of field lines and $P_n^1(\cos\theta)$ the associated Schmidt quasi-normalized Legendre functions of degree n and order 1.

Fig. 1 shows the field lines cut by the magnetopause at apex points for n = 1 to 8. These field lines correspond to the analytical solutions given in Eqs. A(1) to A(8) (see Appendix A) obtained by substituting in Eq. (2) the corresponding associated Schmidt quasi-normalized Legendre functions.

2.2. Determination of the outermost closed field lines

Our second step is to identify the outermost closed lines of the magentic field. For this purpose we consider an idealized magnetopause which, in its delimitation of the field, cuts the lines that cross it and encloses those that do not. The cut lines footprints on the Earth's surface determine the polar caps. Their boundaries, which are also the inner auroral zone bounds, are delineated by the outermost closed line.

According to the constant intensity magnetopause model of Zossi et al. (2020), the magnetic field intensity B^{tot} at every position on this surface has a constant value determined by the solar wind kinetic pressure considered that is on average ~ 50nT in total during quiet solar conditions, of which 25nT are from Earth's core origin. To determine auroral zones outer boundary, that same procedure is followed but considering mean disturbed solar conditions for which the solar wind pressure is balanced by B^{tot} ~ 140-nT (Zossi et al., 2020).

In the axisymmetric configurations considered, for a given closed field line, the lowest magnetic intensity value occurs at its apex. Therefore, the outermost open field line would correspond to that whose intensity at its apex is 25nT. Any other line with apex further than this one is "cut" by the magnetopause and would therefore consitute an open field line. Due to the axisymmetry considered $B_\phi = 0$ everywhere, and in addition at any field line's apex $B_r = 0$. Hence, the value of θ at $r = R_E$ estimated from the field line Eq. (2) that fulfills the condition $B_\theta^{int} = 25$nT at its apex delineates the inner auroral zone boundary, or the polar caps boundary. The same applies for the condition $B_\theta^{int} = 70$nT for the outer boundary. The apex radial distance, r_{apex}, is obtained then from the B_θ equation (given by Eq. (8) of Willis and Young,1987)

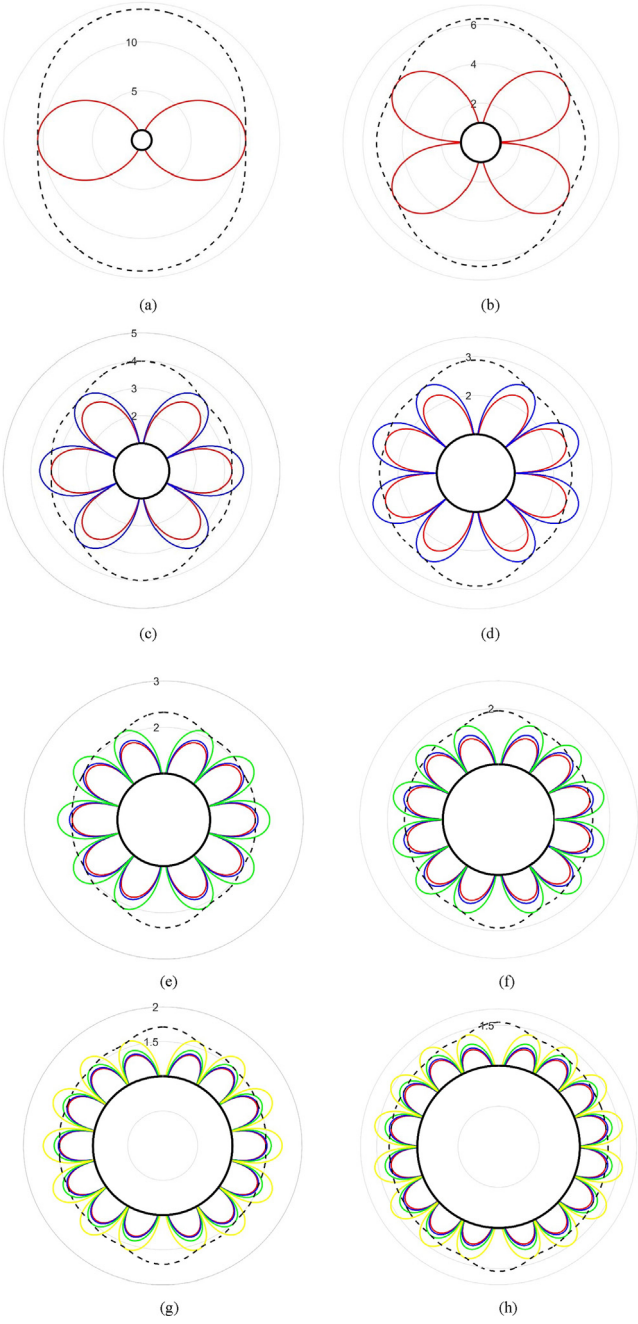

Fig. 1. Meridional cross sections with magnetic field lines cut by the magnetopause at some (or all) apex points for axial harmonics with (a) n = 1, (b) n = 2, (c) n = 3, (d) n = 4, (e) n = 5, (f) n = 6, (g) n = 7, and (h) n = 8. Units are in Earth radius (6371 km). The thick bold solid black circle represents the Earth's surface (note the different scales), and the dashed black line is the magnetopause. In (c) and (d) there are two sets of field lines cut by the magnetopause (red and blue lines). In (e) and (f) there is an additional third line (green line), and in (g) and (h) an additional fourth line (yellow line) cut by the magnetopause. The numbers and the pale blue circles denote different Earth radii (note the different scales in the different subplots). (For interpretation of the references to color in this figure legend, the reader is referred to the web version of this article.)

$$r_{apex} = R_E\left[\left[\frac{1}{2}n(n+1)\right]^{1/2}\frac{g_n^0}{B_\theta}P_n^1(\cos\theta_{apex})\right]^{1/(n+2)} \quad (3)$$

The apex co-latitude angle θ_{apex} corresponds to the roots of $P_n^0(\cos\theta)$. With these two parameters, r_{apex} and θ_{apex}, it is possible to obtain r_n from Eq. (2), which results

$$r_n = \frac{r_{apex}}{\left|\sin\theta_{apex}P_n^1(\cos\theta_{apex})\right|^{1/n}} \quad (4)$$

Thus, the equation of the last closed line is

$$r = \frac{R_E\left[\left[\frac{1}{2}n(n+1)\right]^{1/2}\frac{g_n^0}{B_\theta}P_n^1(\cos\theta_{apex})\right]^{1/(n+2)}}{\left|\sin\theta_{apex}P_n^1(\cos\theta_{apex})\right|^{1/n}}\left|\sin\theta P_n^1(\cos\theta)\right|^{1/n} \quad (5)$$

2.3. Auroral zone latitudinal bounds

The third step is to solve Eq. (5) for θ at $r = R_E$ which delineates the polar cap and auroral zone inner boundary, θ_{in}, for $B_\theta{}^{int} = 25$nT. For the auroral zone outer boundary, θ_{out}, Eq. (5) is solved for $r = R_E$ and $B_\theta^{int} = 70$nT. Hence θ_{in} and θ_{out} are the roots of the following equation:

$$\frac{\left[\left[\frac{1}{2}n(n+1)\right]^{1/2}\frac{g_n^0}{B_\theta}P_n^1(\cos\theta_{apex})\right]^{1/(n+2)}}{\left|\sin\theta_{apex}P_n^1(\cos\theta_{apex})\right|^{1/n}}\left|\sin\theta P_n^1(\cos\theta)\right|^{1/n} = 1 \quad (6)$$

Eq. (6) has n + 1 possible solutions, hence each configuration has n + 1 polar caps. Two of them are true "caps" adjacent to the two geographic poles, so they have one auroral oval each, and the remaining n-1 are band-shaped polar caps with two auroral zones each (one at each boundary), so the total number of auroral ovals is 2n. θ_{in} corresponds to the auroral zone boundary limiting the polar cap, so it serves also as the polar caps' bound, and θ_{out} corresponds to the auroral zone external boundary.

2.4. Setup of axisymmetric Gauss coefficients

For comparison purposes, to determine the axisymmetric Gauss coefficients, g_n^0, we considered a constant field power at the CMB at a distance c = 3480 km from the Earth's center, which is given for a single axial harmonic from Mauersberger–Lowes power spectrum (Lowes, 1974) by

$$R_n = (n+1)\left(\frac{R_E}{c}\right)^{2n+4}\left(g_n^0\right)^2 \quad (7)$$

The axial dipolar coefficient is taken from the International Geomagnetic Reference Field (IGRF version 12) model (Thébault et al., 2015) for the year 2020, so that $|g_1^0|$=29404.8 nT and in the purely axial dipolar case $R_1 = 6.51 \times 10^{10}$ nT^2. The other Gauss coefficients, listed in Table 1, are calculated from Eq. (7) with this R_1 value. This constant power principle corresponds to a reversal characterized by energy cascading from the dipole to higher degrees (Amit and Olson, 2010).

Fig. 2 shows the resulting $|g_n^0|$ together with the mean magnetopause distance for each n obtained from the constant intensity magnetopause model during quiet solar wind conditions. A magnetopause approach is clearly noticed for increasing n. An estimate of the mean magnetopause distance could be obtained using Eq. (3) for r_{apex},

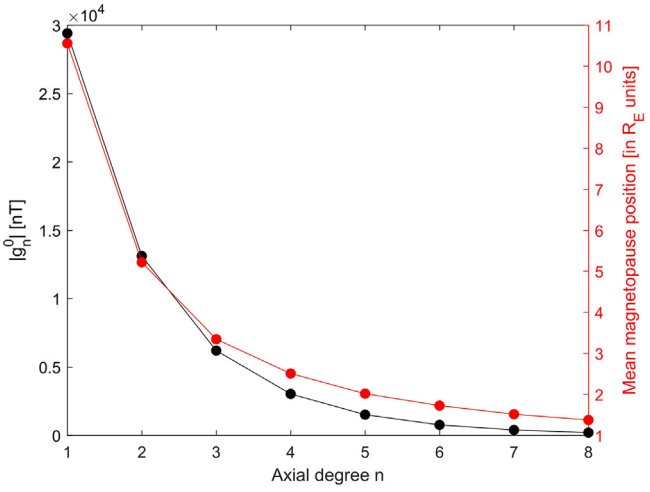

Fig. 2. Gauss coefficient $|g_n^0|$ of the single harmonic axial field (black) and mean magnetopause position (red) vs. degree n. (For interpretation of the references to color in this figure legend, the reader is referred to the web version of this article.)

Table 1
Setup of Gauss coefficients in nT, resulting number of polar caps and auroral zones, and their total area in % of the Earth's surface area for each axial degree from n = 1 to 8.

Degree n	Gauss coefficient $\|g_n^0\|$ in nT	Number of polar caps	Polar caps total area in % of Earth's surface	Number of auroral zones	Auroral zones total area in % of Earth's surface
1	29404.8	2	4.85	2	2.23
2	13114.3	3	2.13	4	1.57
3	6203.6	4	1.61	6	1.51
4	3030.8	5	1.62	8	1.75
5	1511.3	6	1.93	10	2.30
6	764.3	7	2.56	12	3.28
7	390.5	8	3.63	14	4.93
8	201.1	9	5.44	16	7.75

replacing g_n^0 by its expression from Eq. (7), approximating $R_1^{1/2}/B_\theta$ by 10^4, and considering that the mean square root value of $P_n^1(\cos\theta)$ is $[4\pi(2n + 1)]^{-1/2}$. The mean magnetopause distance would vary then as $\{10^8 n/[4\pi(2n + 1)]\}^{1/(2n+4)}$, which is roughly equivalent to $(10^8/4\pi)^{1/(2n+4)}$.

3. Results

Fig. 1 shows a meridian projection of the magnetic field closed lines cut by the magnetopause at apex points (that is the last magnetic field closed line) and the magnetopause position that is an isoline of internal magnetic field intensity equal to 25nT, for different degrees of single harmonic axial fields. A magnetic field line, given by Eq. (5) for a given r_{apex}, appears in Fig. 1 as a set of n lobes drawn with the same color. Thus, the red, blue, green and yellow lines are four different outermost closed field lines which have some of their n lobes cut the magnetopause. Not all, because not all lobes' apex have $B_\theta^{int} = 25$ nT. Those cut lobes' footprints delineate the polar caps at Earth's surface. In the dipole and quadrupole cases there is a single line (red line in Fig. 1(a) and (b)), which corresponds to a single r_{apex} value, which is cut by the magnetopause at all its lobes. In fact, the number of lines is one for n = 1 and 2, two for n = 3 and 4, three for n = 5 and 6, and four for n = 7 and 8. For example, in the case of n = 8, at the right (or left) sides of Earth's meridian, the red line is cut by the magnetopause at the pair of lobes near the equator but not at the remaining six. The blue line, which has a different r_{apex}, is cut at the four low-latitude lobes, while the green line is cut at all lobes except the two near the geographic poles, and the yellow line at all lobes.

Polar caps and auroral zones are shown in Fig. 3. Their number increases with n as can be clearly observed in this figure and in Table 1.

The polar cap and auroral zone total areas as functions of n are listed in Table 1 and plotted in Fig. 4. It is clearly observed that, even though the number of polar caps and consequently of auroral zones increase with increasing n, the total areas exhibit a more complex behavior. Both areas decrease first, reaching a minimum at n = 3, and from thereafter increase. However, the area increasing rate is much higher in the auroral zone case which exceeds the dipolar value at n = 5 while in the polar caps case this occurs only at n = 8 (Fig. 4). In contrast, the decrease from the dipole to n = 3 is more than twice larger in the case of the polar caps area (Fig. 4).

Systematic analysis of the polar caps and auroral zones boundaries location is more complex, since we have, as already mentioned, different types. In the case of the polar caps (n + 1 in total per configuration) only two are "true" caps adjacent to each geographic pole, and the remaining n-1 band-shaped caps appear at lower latitudes. In the case of even n, one of these band-shaped polar caps surrounds the equator. Of the 2n auroral zones there are two, one at each hemisphere, encircling the polar caps adjacent to the geographic poles, and the remaining 2n-2 are distributed two per band-shaped polar cap, as can be noticed in Fig. 3.

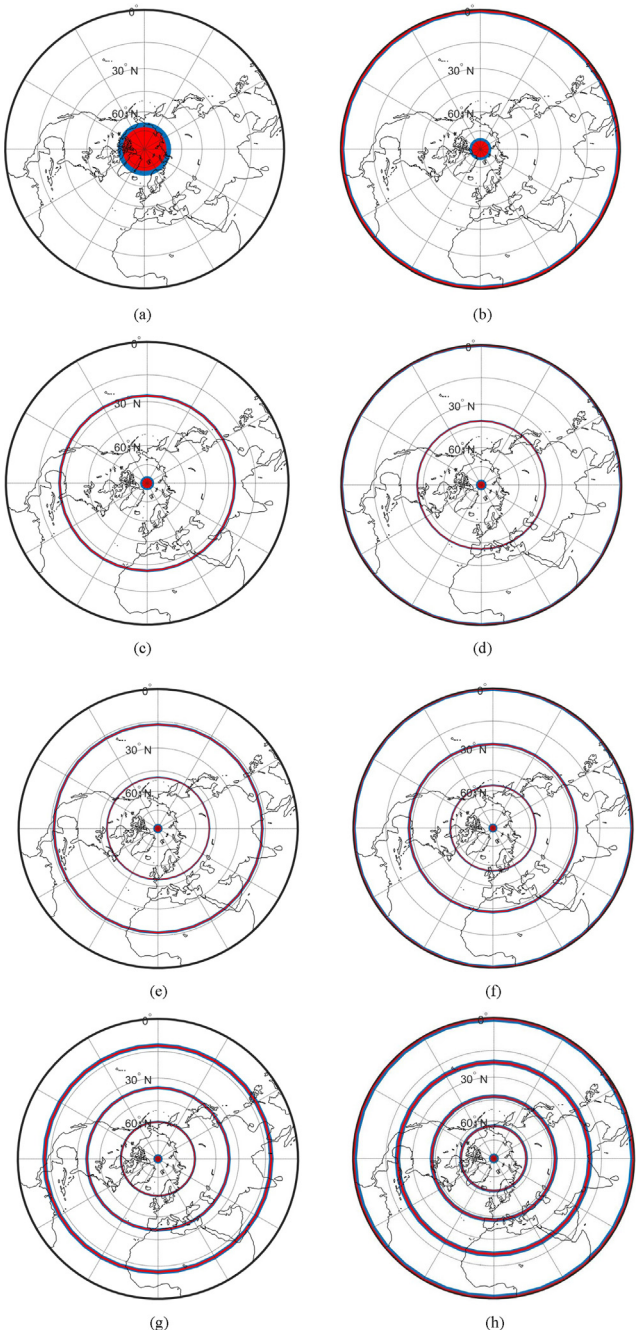

Fig. 3. Polar caps (red shaded areas) and auroral zones (blue shaded areas) for single harmonic axial fields with (a) n = 1, (b) n = 2, (c) n = 3, (d) n = 4, (e) n = 5, (f) n = 6, (g) n = 7, and (h) n = 8, for the northern hemisphere. (For interpretation of the references to color in this figure legend, the reader is referred to the web version of this article.)

Fig. 5. Shows the latitudes of the inner and outer boundaries λ_{in} and λ_{out} for the auroral zones adjacent to the polar caps at the geographic poles, which can be directly compared. As expected, both boundaries move to higher latitudes as n increases from 1 to 6. From n = 6 to 8, λ_{in} and λ_{out} exhibit nearly constant values very close to the

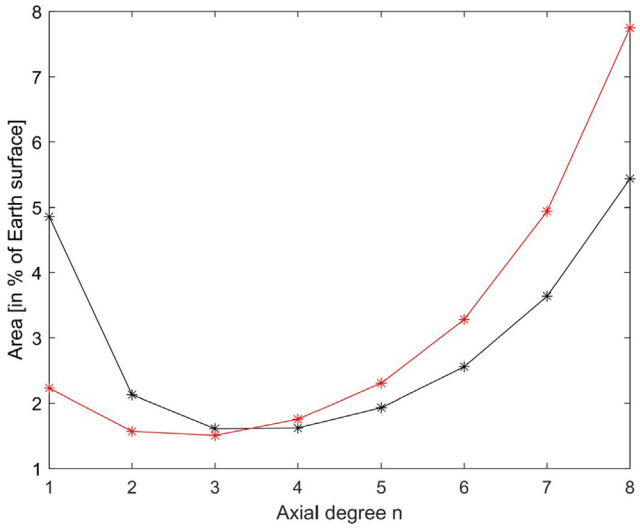

Fig. 4. Total area in % of Earth's surface area ($4\pi R_E^2$) of polar caps (black) and auroral zones (red) vs. the degree n of the single axial harmonic. (For interpretation of the references to color in this figure legend, the reader is referred to the web version of this article.)

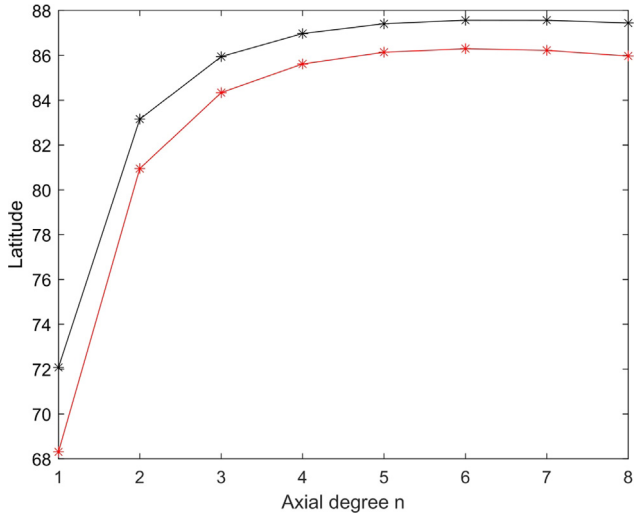

Fig. 5. Latitudes of inner (black) and outer (red) boundaries of auroral zones around the polar caps that are adjacent to the geographic poles vs. the degree n of the single axial harmonic. (For interpretation of the references to color in this figure legend, the reader is referred to the web version of this article.)

geographical poles. For much larger n values the corresponding lobes closer to the geographic poles fulfill the condition of $B_\theta^{int} = 25nT$ at their apices for $r_{apex} < 1$, i.e. below Earth's surface. Such high degrees were not analyzed in the present work.

4. Discussion and conclusions

Obviously, any geomagnetic field, including the transitional reversing field, is multi-harmonic with non-axial contributions. Nevertheless, in the context of the impact of the geomagnetic field on polar caps and auroral zones, considering single harmonic axial fields may be useful for several reasons. First, exact analytical solutions can be obtained. Second, a reversal is by definition the collapse of the axial dipole, i.e. it is defined by an axial single harmonic. Third, the present-day field (and possibly the past paleomagnetic field too, see e.g. Merrill et al., 1998) is strongly dominated by the axial dipole single harmonic. Finally, in general, considering single harmonics may provide useful fundamental physical understanding. In the context of geomagnetism, this is common practice. A few examples include: modelling of heterogeneous boundary control on planetary dynamos using single harmonic CMB heat flux for the Earth (e.g. Glatzmaier et al., 1999; Olson and Christensen, 2002; Aubert et al., 2007; Olson et al., 2010; Sahoo et al., 2016; Mound et al., 2019) as well as for Mars (Stanley et al., 2008; Amit et al., 2011; Dietrich and Wicht, 2013), Mercury (Cao et al., 2014) and Saturn (Stanley, 2010) or using single harmonic inner core boundary buoyancy flux (Aubert et al., 2013); using single harmonic core flows for kinematic modelling of energy transfer on the CMB (e.g. Huguet et al., 2016), local time series of the surface field (e.g. Trindade et al., 2018) or geomagnetic jerks (Pinheiro et al., 2019).

Our results show that the polar cap and auroral zone areas are highly sensitive to B_θ, their dependence on n is similar for any pair of solar wind conditions. As n increases the areas first decrease, but from $n = 3$ they begin to increase surpassing their dipolar values. Non-dipolar axial fields, as those here analyzed may emerge while the dipole collapses in a reversal. In fact, during the past 120 years based on the IGRF 12 core field model (Thébault et al., 2015), all the axial non-dipole geomagnetic field harmonics have been increasing in parallel with the decrease of the axial dipole (Fig. 6).

Fig. 5 implies that polar caps adjacent to geographic poles shrink with increasing axial degree, at least up to $n = 6$–7. If instead of increasing axial degree we would

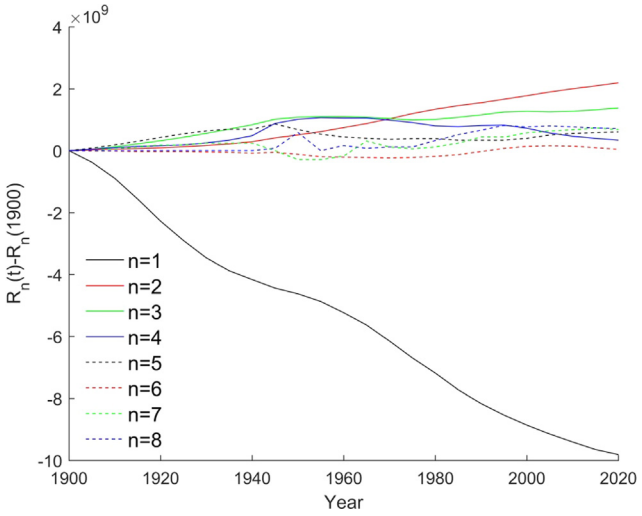

Fig. 6. Field power at the core-mantle boundary for each single harmonic axial degree (see legend) with respect to its 1900 value until present using Gauss coefficients from IGRF (version 12).

have considered a single axial dipolar field with an always decreasing moment, these polar caps would have increased monotonously, as expected (Siscoe and Chen, 1975; Vogt and Glassmeier, 2001; Glassmeier et al., 2004). This indicates a fundamental difference between the impact of dipole collapse and energy cascade reversal scenarios on the auroral zones in the polar regions. In the dipole collapse scenario these "true" polar cap areas increase, whereas with energy cascade the areas shrink. Of course, the overall situation with high axial degrees is that lower latitude polar caps appear, adding to the total polar caps area hence increasing the polar caps and auroral zones total area.

For tilted single degree fields the same configuration of polar caps and auroral zones as in the axial cases would hold but this time centered at the corresponding magnetic poles, i.e. still antipodal but not coincident with the geographic poles. This would imply that, for example in the most extreme case of an axis in the geographic equatorial plane (as in the dipolar rotation reversal scenario analyzed in Zossi et al., 2019), at a certain local time polar caps and auroral zones would face the sun in all their extent, whereas 12 h later they would be completely in shadow. In addition, aurorae would be observed exclusively in specific longitudes if tilted fields prevail.

To our best knowledge, there is no analytical solution to magnetic field lines with several axial degrees. The non-linearity of the equations prohibits a solution in the form of e.g. linear superposition of single axial harmonic solutions. However, taking into account that the field intensity decreases with $1/r^{n+2}$, the number of polar caps and auroral zones would be mainly determined by the lowest dominant degree. During a dipole decay event, positive and negative contributions of the higher degree non-axial harmonics may lead to loss of north–south symmetry. This is the case of the auroral zone area secular variation during the past 120 years analyzed in Zossi et al. (2020), where the non-dipolar components counteract and exceed the increasing polar cap area trend induced by the dipolar moment decrease in the northern hemisphere, while enhancing the increasing polar cap area trend in the southern hemisphere.

Our results suggest that during reversals new auroral zones and polar caps emerge at low latitudes. If the axial dipole energy is transferred to high axial degrees the total areas of auroral zones and polar caps are expected to exceed those of the present-day axial dipole dominated field, but these auroral zones are distributed at different latitudes. In addition, the polar caps adjacent to the geographical poles are expected to reach very close to the geographical poles. If the transitional field contains significant non-axial contributions, the auroral zones appear at specific longitudes. In the reversal scenarios studied by Zossi et al. (2019), four small-scale polar caps emerge at different latitudes and longitudes, testimony for the dominance of multiple quadrupole orders in the absence of the decaying dipole.

The magnetopause approach that we use, combined with any field, allows to obtain results in first approximation, which cannot be obtained easily with more accurate magnetosphere models, using for example magnetohydrodynamic considerations. Although our results cannot be directly applied to the multi-harmonic geomagnetic field, the advantages of analytical solutions such as those applied in this study are the simplicity and fast computation which allow for fundamental understanding of the relation between a component of the geomagnetic core field morphology and Earth regions which are more exposed to energetic particles and aurorae occurrences.

Declaration of Competing Interest

The authors declare that they have no known competing financial interests or personal relationships that could have appeared to influence the work reported in this paper.

Acknowledgements

B.S. Zossi and A.G. Elias acknowledge financial support from Projects PICT 2015-0511, PIUNT E642 and PIP 294/14. IGRF is freely available at https://www.ngdc.noaa.gov/IAGA/vmod/igrf.html. We thank three anonymous reviewers for their constructive reviews.

Appendix A. Substituting the associated Schimdt quasi-normalized Legendre functions in Eq. (2), the magnetic field lines equations for n = 1 to 8 are the following

$$n = 1 : r = r_1(\sin\theta)^2 \tag{A1}$$

$$n = 2 : r = r_2\left|\sqrt{3}(\sin\theta)^2\cos\theta\right|^{1/2} \tag{A2}$$

$$n = 3 : r = r_3\left|\frac{\sqrt{6}}{4}(\sin\theta)^2\left(5cos^2\theta - 1\right)\right|^{1/3} \tag{A3}$$

$$n = 4 : r = r_4\left|\frac{\sqrt{10}}{4}(\sin\theta)^2\cos\theta\left(7cos^2\theta - 3\right)\right|^{1/4} \tag{A4}$$

$$n = 5 : r = r_5\left|\frac{\sqrt{15}}{8}(\sin\theta)^2\left(21cos^4\theta - 14cos^2\theta + 1\right)\right|^{1/5} \tag{A5}$$

$$n = 6 : r = r_6\left|\frac{\sqrt{21}}{18}(\sin\theta)^2\cos\theta\left(33cos^4\theta - 30cos^2\theta + 5\right)\right|^{1/4} \tag{A6}$$

$$n = 7 : r = r_7\left|\frac{\sqrt{7}}{32}(\sin\theta)^2\left(429cos^6\theta - 495cos^4\theta + 135cos^2\theta - 5\right)\right|^{1/5} \tag{A7}$$

$$n = 8 : r = r_8 \left| \frac{1}{32} (\sin\theta)^2 \cos\theta \left(2145 cos^6\theta - 3003 cos^4\theta + 1155 cos^2\theta - 105\right) \right|^{1/5} \quad \text{(A8)}$$

References

Akasofu, S.-I., 1983. Evolution of ideas in solar-terrestrial physics. Geophys. J. R. Astron. Soc. 74 (1), 257–299. https://doi.org/10.1111/j.1365-246X.1983.tb01880.x.

Alexeev, I.I., 2005. What Defines the Polar Cap and Auroral Oval Diameters?, in The Inner Magnetosphere: Physics and Modeling, Editors: Pulkkinen, T.I., N.A. Tsyganenko & R.H.W Friedel. American Geophysical Union, Geophysical Monograph 155, 257–262.

Amit, H., Christensen, U.R., Langlais, B., 2011. The influence of degree-1 mantle heterogeneity on the past dynamo of Mars. Phys. Earth Planet. Inter. 189 (1-2), 63–79. https://doi.org/10.1016/j.pepi.2011.07.008.

Amit, H., Leonhardt, R., Wicht, J., 2010. Polarity reversals from paleomagnetic observations and numerical dynamo simulations. Space Sci. Rev. 155, 293–335.

Amit, H., Olson, P., 2008. Geomagnetic dipole tilt changes induced by core flow. Phys. Earth Planet. Inter. 166 (3-4), 226–238. https://doi.org/10.1016/j.pepi.2008.01.007.

Amit, H., Olson, P., 2010. A Dynamo Cascade Interpretation of the Geomagnetic Dipole Decrease. Geophys. J. Int. 181, 1411–1427. https://doi.org/10.1111/j.1365-246X.2010.04596.x.

Aubert, J., Amit, H., Hulot, G., 2007. Detecting thermal boundary control in surface flows from numerical dynamos. Phys. Earth Planet. Inter. 160 (2), 143–156.

Aubert, J., Finlay, C.C., Fournier, A., 2013. Bottom-up control of geomagnetic secular variation by the Earth's inner core. Nature 502 (7470), 219–223. https://doi.org/10.1038/nature12574.

Beard, D.B., 1960. Interaction of the solar plasma with the Earth's magnetic field. Phys. Rev. Lett. 5 (3), 89–91. https://doi.org/10.1103/PhysRevLett.5.89.

Cao, H., Aurnou, J.M., Wicht, J., Dietrich, W., Soderlund, K.M., Russell, C.T., 2014. A dynamo explanation for Mercury's anomalous magnetic field. Geophys. Res. Lett. 41, 4127–4134, https://doi.org/doi:10.1002/2014GL060196.

Chapman, S., Ferraro, V.C.A., 1931. A new theory of magnetic storms. Terr. Magn. Atmos. Electr. 36, 77–97. https://doi.org/10.1029/TE036i002p00077.

Christensen, U.R., Aubert, J., Hulot, G., 2010. Conditions for Earth-like geodynamo models. Earth Planet. Sci. Lett. 296 (3-4), 487–496.

Dietrich, W., Wicht, J., 2013. A hemispherical dynamo model: Implications for the Martian crustal magnetization. Phys. Earth Planet. Inter. 217, 10–21. https://doi.org/10.1016/j.pepi.2013.01.001.

Glassmeier, K.H., Vogt, J., Stadelmann, A., Buchert, S., 2004. Concerning long-term geomagnetic variations and space climatology. Ann. Geophys. 22, 3669–3677. https://doi.org/10.5194/angeo-22-3669-2004.

Glatzmaier, G.A., Coe, R.S., Hongre, L., Roberts, P.H., 1999. The role of the Earth's mantle in controlling the frequency of geomagnetic reversals. Nature 401 (6756), 885–890. https://doi.org/10.1038/44776.

Feldstein, Y.I., 2016. The discovery and the first studies of the auroral oval: A review. Geomag. Aeron. 56 (2), 129–142. https://doi.org/10.1134/S0016793216020043.

Finlay, C.C., 2008. Historical variation of the geomagnetic axial dipole. Phys. Earth Planet. Inter. 170 (1-2), 1–14. https://doi.org/10.1016/j.pepi.2008.06.029.

Huguet, L., Amit, H., Alboussière, T., 2016. Magnetic to magnetic and kinetic to magnetic energy transfers at the top of the Earth's core. Geophys. J. Int. 207 (2), 934–948. https://doi.org/10.1093/gji/ggw317.

Lowes, F.J., 1974. Spatial Power Spectrum of the Main Geomagnetic Field, and Extrapolation to the Core. Geophys. J. R. Astron. Soc. 36 (3), 717–730. https://doi.org/10.1111/j.1365-246X.1974.tb00622.x.

Merrill, R.T., McFadden, P.L., 1999. Geomagnetic polarity transitions. Rev. Geophys. 37, 201–226, https://doi.org/:10.1029/1998RG900004.

Merrill, R., McElhinny, M., McFadden, P., 1998. The Magnetic Field of the Earth: Paleomagnetism, the Core, and the Deep Mantle. Academic Press, San Diego.

Milan, S.E., 2009. Both solar wind-magnetosphere coupling and ring current intensity control of the size of the auroral oval. Geophys. Res. Lett. 36, L18101. https://doi.org/10.1029/2009GL039997.

Mound, J., Davies, C., Rost, S., Aurnou, J., 2019. Regional stratification at the top of Earth's core due to core–mantle boundary heat flux variations. Nat. Geosci. 12 (7), 575–580. https://doi.org/10.1038/s41561-019-0381-z.

Olson, P., Christensen, U.R., 2002. The time-averaged magnetic field in numerical dynamos with non-uniform boundary heat flow. Geophys. J. Int. 151 (3), 809–823. https://doi.org/10.1046/j.1365-246X.2002.01818.x.

Olson, P.L., Coe, R.S., Driscoll, P.E., Glatzmaier, G.A., Roberts, P.H., 2010. Geodynamo reversal frequency and heterogeneous core-mantle boundary heat flow. Phys. Earth Planet. Inter. 180 (1-2), 66–79.

Pinheiro, K.J., Amit, H., Terra-Nova, F., 2019. Geomagnetic jerk features produced using synthetic core flow models. Phys. Earth Planet. Inter. 291, 35–53. https://doi.org/10.1016/j.pepi.2019.03.006.

Sahoo, S., Sreenivasan, B., Amit, H., 2016. Dynamos driven by weak thermal convection and heterogeneous outer boundary heat flux. Phys. Earth Planet. Inter. 250, 35–45. https://doi.org/10.1016/j.pepi.2015.11.003.

Siscoe, G.L., Chen, C.-K., 1975. The paleomagnetosphere. J. Geophys. Res. 80 (34), 4675–4680. https://doi.org/10.1029/JA080i034p04675.

Siscoe, G.L., Sibeck, D.G., 1980. Effects of nondipole components on auroral zone configurations during weak dipole field epochs. J. Geophys. Res. 85 (B7), 3549–3556. https://doi.org/10.1029/JB085iB07p03549.

Smith, A.R.A., Beggan, C.D., Macmillan, S., Whaler, K.A., 2017. Climatology of the auroral electrojets derived from the along-track gradient of magnetic field intensity measured by POGO, Magsat, CHAMP, and Swarm. Space Weather 15 (10), 1257–1269. https://doi.org/10.1002/2017SW001675.

Stanley, S., Elkins-Tanton, L., Zuber, M.T., Parmentier, E.M., 2008. Mars' paleomagnetic field as the result of a single-hemisphere dynamo. Science 321 (5897), 1822–1825. https://doi.org/10.1126/science:1161119.

Stanley, S., 2010. A dynamo model for axisymmetrizing Saturn's magnetic field. Geophys. Res. Lett. 37 (5), n/a–n/a.

Thébault, E., Finlay, C.C., Beggan, C.D., Alken, P., Aubert, J., Barrois, O., Bertrand, F., Bondar, T., Boness, A., Brocco, L., Canet, E., Chambodut, A., Chulliat, A., Coïsson, P., Civet, F., Du, A., Fournier, A., Fratter, I., Gillet, N., Hamilton, B., Hamoudi, M., Hulot, G., Jager, T., Korte, M., Kuang, W., Lalanne, X., Langlais, B., Léger, J.-M., Lesur, V., Lowes, F.J., Macmillan, S., Mandea, M., Manoj, C., Maus, S., Olsen, N., Petrov, V., Ridley, V., Rother, M., Sabaka, T.J., Saturnino, D., Schachtschneider, R., Sirol, O., Tangborn, A., Thomson, A., Tøffner-Clausen, L., Vigneron, P., Wardinski, I., Zvereva, T., 2015. International Geomagnetic Reference Field: the 12th generation. Earth Planets Space 67 (1). https://doi.org/10.1186/s40623-015-0228-9.

Trindade, R.I.F., Jaqueto, P., Terra-Nova, F., Brandt, D., Hartmann, G.A., Feinberg, J.M., Strauss, B.E., Novello, V.F., Cruz, F.W., Karmann, I., Cheng, H., Edwards, R.L., 2018. Speleothem record of geomagnetic South Atlantic Anomaly recurrence. PNAS 115 (52), 13198–13203. https://doi.org/10.1073/pnas.1809197115.

Tsyganenko, N.A., 2019. Secular drift of the auroral ovals: How fast do they actually move?. Geophys. Res. Lett. 46 (6), 3017–3023. https://doi.org/10.1029/2019GL082159.

Vogt, J., Glassmeier, K.-H., 2001. Modelling the paleomagnetosphere: strategy and first results. Adv. Space Res. 28 (6), 863–868. https://doi.org/10.1016/S0273-1177(01)00504-X.

Willis, D.M., Young, L.R., 1987. Equation for the field lines of an axisymmetric magnetic multipole. Geophys. J. Int. 89 (3), 1011–1022.

https://doi.org/10.1111/gji.1987.89.issue-310.1111/j.1365-246X.1987.tb05206.x.

Zossi, B.S., Fagre, M., Amit, H., Elias, A.G., 2019. Polar caps during geomagnetic polarity reversals. Geophys. J. Int. 216, 1334–1343. https://doi.org/10.1093/gji/ggy494.

Zossi, B., Fagre, M., Amit, H., Elias, A.G., 2020. Geomagnetic field model indicates shrinking northern auroral oval. Journal of Geophysical Research, 125, e2019JA027434. https://doi.org/10.1029/2019JA027434.